



Cyclic damage quantification in composite materials using discrete damage mechanics

Nikolay V. Turbin^{a,*}, Kirill A. Shelkov^c, Nikolay O. Kononov^a, Ever J. Barbero^b

^a Institute N^o14, Moscow Aviation Institute, Volokolamskoe shosse, 4, Moscow 125993, Russia

^b Mechanical and Aerospace Engineering, West Virginia University, Morgantown, WV, USA

^c Moscow Aviation Institute, Aerospace Engineering Department, Volokolamskoe shosse, 4, Moscow 125993, Russia

ARTICLE INFO

Keywords:

Discrete damage mechanics
Polymer composite materials
Fatigue cycle
Crack density
Fracture toughness
Laminate
Matrix

ABSTRACT

A method for fatigue damage quantification in composite materials, based on experimental stiffness degradation data for composite laminates subjected to cyclic load is proposed. Discrete damage mechanics theory is used to calculate crack density vs. number of cycles from elastic moduli-reduction data obtained during fatigue experiments. The calculated crack density simplifies fatigue testing by diminishing the need for counting cracks during testing. Accurate results are achieved and reported. The defect-nucleation rate, which controls the fatigue damage rate, is also obtained from processing the modulus-reduction data. It is observed that the defect-nucleation rate has a small scatter and is independent of applied load magnitude. Furthermore, the onset of delamination observed in the experiments correlates very well with the onset of deviation between the predicted and experimental curves of elastic moduli-reduction versus accumulated crack density. An additional parameter, the defect-nucleation threshold, is here proposed to further characterize the fatigue performance of the composite material under stress-controlled fatigue loading, in contrast to thermal fatigue results from the literature. Furthermore, the difference in damage nucleation rate between strain-controlled and stress-controlled was observed and discussed.

1. Introduction

Polymer composite materials (PCM) have become popular for weight-sensitive applications such as aerospace, automotive, marine, sport, and others. Meanwhile, for the PCM structures to be cost-competitive, reliable, and as safe as those fabricated using traditional materials, such as metals, it is necessary to develop reliable methods for predicting the behavior of PCM structures so that they can be efficiently designed [1]. Such methods must include the quantification of the changes in the material that occur during service, such as damage accumulation.

From a strength and fracture toughness point of view, the weak link of PCM is the matrix, with matrix cracking being the dominant early form of damage, which is the precursor for other, more severe forms of damage, such as fiber breaks and delaminations. The role of matrix cracking is even more critical when the structure is subjected to long-term cyclic loading under various environmental conditions. For example, moisture condensation may contribute to damage accumulation and consequent loss of hermeticity [2,3]. On the other hand,

conventional in-service methods for damage detection, such as non-destructive evaluation (NDE), may be ineffective for matrix cracking monitoring because the crack planes are normal to the laminate surface, and thus difficult to detect with NDE techniques [4,5].

Experimental work and associated models for predicting matrix cracking in carbon-fiber reinforced plastics (CFRP) have been reported [6–11]. In those, one of the key features regarding the appearance and accumulation of matrix cracking was found to be its regularity, i.e., vertical through-layer-thickness cracks are positioned evenly, and the rate of crack's propagation in the thickness direction is nearly instantaneous [12]. This observation served as a reasonable and fruitful hypothesis, later implemented in damage mechanics models. Models developed based on direct (visual) observations of defect-progression have shown to be very accurate [13–21].

Due to the cost and difficulties of parameter identification, models that require a single material property to predict both initiation and rate are advantageous. For example, mode I intra-ply fracture toughness has been shown to be very effective in predicting a wealth of experimental data [16,18,19,23]. To validate model predictions, measurement of crack densification has been reported. For example, with X-ray

* Corresponding author.

E-mail addresses: turbinnv@mai.ru (N.V. Turbin), kononovno@mai.ru (N.O. Kononov), ever.barbero@mail.wvu.edu (E.J. Barbero).

<https://doi.org/10.1016/j.compstruct.2024.118271>

Received 26 January 2024; Received in revised form 19 April 2024; Accepted 6 June 2024

Available online 7 June 2024

0263-8223/© 2024 Elsevier Ltd. All rights reserved, including those for text and data mining, AI training, and similar technologies.

Nomenclature	
<i>List of symbols:</i>	
λ	crack density, mm^{-1}
G_I	energy release rate, N/mm
G_{Ic}	critical value of energy release rate, initial fracture toughness, N/mm
G'_{Ic}	fatigue fracture toughness, N/mm
l	half distance between cracks
$\hat{\varepsilon}_x$	average laminate deformation
$\hat{\sigma}_x$	stress applied to the boundary of the RVE
$u_0(x)$	fundamental homogenous solution
$u_i^l(x, z)$	perturbations produced by the intralaminar cracks
τ_{xz}	interlaminar stresses
$[A]$	eigenvalues
$[V]$	eigenvectors
δ_{js}	Kronecker delta
$f(N)$	defect-nucleation function
β	defect-nucleation rate
E_{x0}	initial longitudinal elastic modulus, MPa
E_x	fatigue longitudinal elastic modulus, MPa
E_x^{exp}	longitudinal elastic modulus from experiment
E_x^{DDM}	longitudinal elastic modulus obtained with DDM
N	cycle number
R	mean squared error

contrasting methods [20,21,24,25], acoustic emissions [11,24,26], tomography [9], automated image processing [7,8], and so on.

One such model, discrete damage mechanics (DDM) [18], has been validated with experimental data from quasi-static mechanical-loading tests on several material systems and laminate stacking sequences (LSS). DDM is a synergistic method, combining analytical micromechanics of damage at the lamina-level with continuum damage mechanics at the laminate-level to predict damage initiation and evolution as a function of applied strain using a single material property, i.e., the fracture toughness G_{Ic} of the lamina, which is measured by matching the predicted with the measured crack density as a function of strain.

The extension of DDM for fatigue requires an additional parameter, i.e., the defect-nucleation ratio, which was obtained using data from thermal-fatigue tests [27, Ch. 11]. The validation of the DDM framework [16–18] for mechanical fatigue has not been studied yet. Such validation requires measuring crack-density accumulation and laminate stiffness reduction as a function of the number of cycles.

There are different approaches for crack density measuring during fatigue testing. The in-situ method typically employs a camera to capture the edges of the specimen, that are painted in white color before testing, to provide better contrast for cracks visualization [7,8]. The method is convenient, but the damage state on the edges might not be the same as the damage state in the interior section of the specimen, so crack density value may become ill-informed in this case.

Meanwhile, it is reported that when the cracking lamina is sufficiently thick, cracks from the edges immediately span all the width of the specimen and thus, there are equal crack densities on the edges and in the central part of the specimen [7,8]. Full field fatigue cracking detection in a specimen is often done by tomography, which necessitates multiple removals of the specimen from the testing device. The ex-situ measuring of the internal damage by tomography has been shown to affect the posterior accumulation of cracks during loading and fatigue life [28,29].

In contrast to physically based models, such as DDM [18], phenomenological models circumvent the need for non-destructive crack-density extraction during fatigue testing by relying on residual strength or residual stiffness measurements as a function of number of fatigue cycles [30–33,38,39]. For the residual-stiffness model, obtaining the empirical relationship between elastic properties and the number of load cycles requires a set of typical strain-measurement devices, such as strain gauges, extensometers, optical strain sensors, etc. [34,35]. The thus obtained dependencies give approximated laws of stiffness degradation described by several empirical parameters.

The required data for phenomenological fatigue damage models is easy to collect, but the more universal and accurate the model is, the more experiments it requires, which results in massive testing campaigns. See for example [36]. It must be noted that parameter identification may require new or additional testing for each material system

and each laminate stacking sequence (LSS).

This work proposes a method, using only stiffness degradation data, to obtain the damage and fatigue properties needed for physically based fatigue models such as DDM [18]. The proposed framework employs analytical DDM equations combined with residual fracture toughness equations. A Nelder-Mead [37] minimization algorithm is used to obtain the fatigue properties from standard stiffness-degradation experimental data. The proposed methodology is demonstrated using fatigue data from the literature [7,8].

2. Discrete damage mechanics

The objective of this section is to present the equations used to calculate the reduced modulus E_x as a function of crack density λ . The equations are then used to fit experimental $\frac{E_x}{E_{x0}}(\lambda)$ data and thus to obtain the crack density corresponding to each experimental value of E_x . Specifically, the crack density corresponding to each experimental value of E_x is calculated. It is then possible to use another equation to calculate the Energy Release Rate (ERR, G_I) as a function of crack density λ that allows such values of crack density to occur. Furthermore, the calculated ERR G_I , which decreases with the number of cycles, can then be used to calculate the defect-nucleation function $f(N)$ that characterizes the fatigue phenomenon. Additionally, when deviations from calculated vs. experimental modulus data are noted, it is possible to detect when delaminations appear.

The scope of the present study includes symmetrical, balanced laminates, subjected to in-plane load. It is shown elsewhere [12,16,19], that for such a case, matrix cracks grow parallel to the fiber direction, and they are approximately equally spaced. Thus, it is assumed that the cracks are spaced regularly. This allows us to consider a representative volume element (RVE) of the laminate region between neighboring cracks. The crack density in the lamina is defined as:

$$\lambda_i = \frac{1}{2l} \tag{1}$$

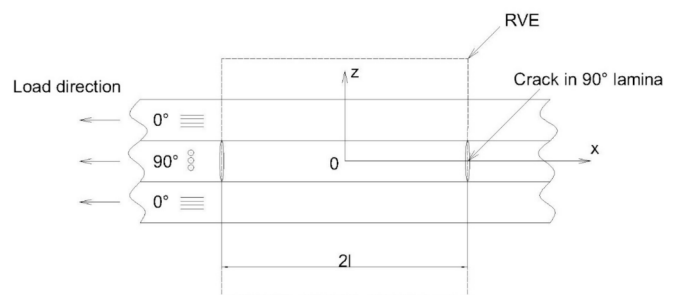


Fig. 1. RVE with cracks [16].

where $2l$ is the distance between cracks. (Fig. 1) shows the RVE with dimension $2l \times 2h \times 1$, where $2h$ – the thickness of laminate.

The initial value of crack density λ_i is assumed to be a small value about 0.01 mm^{-1} . The inclusion of such initial defects is justified by the physical material state after fabrication, where some small defects are always present. Also, the computational model of DDM doesn't work without any crack density prescribed. The initial crack density doesn't affect elastic modulus, which is verified by comparison of DDM predictions to CLT result for E_x modulus.

In case of pure mechanical loading (temperature increment is absent: $\Delta T = 0$), the unit stress applied on the boundary of the RVE $\hat{\sigma}_x = 1$ serves to find the effective elastic moduli of the laminate E_x as a function of the crack density λ_i [16]:

$$E_x = \frac{1}{\hat{\varepsilon}_x} \quad (2)$$

$$\hat{\varepsilon}_x = \frac{\hat{u}(l)}{l} \quad (3)$$

where $\hat{\varepsilon}_x$ is average laminate deformation, resulting from a unit stress $\hat{\sigma}_x = 1$ applied at the boundary of the RVE, and $\hat{u}(l)$ is the average displacement on the boundary of RVE. The average displacement calculation is based on following assumptions:

1. Lines initially normal to the middle surface remain incompressible ($\varepsilon_z = 0$).
2. Small deformations and infinitesimal strains.
3. For narrow plates and beams, $\sigma_y = 0$.

Taking all these assumptions together, results in the following kinematics:

$$\begin{cases} u^i = u^i(x, z) = u_0(x) + u_1^i(x, z) \\ v^i = 0, \text{ or } v^i = v_0(y) \\ w^i = 0 \end{cases} \quad (4)$$

where $u_0(x)$ is the fundamental homogenous solution and $u_1^i(x, z)$ are perturbations produced by the intralaminar cracks.

Next, it is possible to calculate the displacements (4) using a 1D formulation, which allows for an analytical solution for all the unknowns. If one lamina is damaged, the stress on other laminas should increase. At the same time, at both ends of the RVE (Fig. 1), the cracked lamina does not carry axial stress. However, due to the bonding with other laminas, interlaminar stresses τ_{xz} appear to ensure continuity of displacements at the interface between laminas. For a symmetric laminate, the displacements must be symmetric. The interlaminar stresses

must be antisymmetric with respect to the middle surface and null at the middle surface (Fig. 2). The interlaminar stresses are assumed to be linear across the thickness, so the average displacement depends on a single independent variable x . However, interlaminar stresses can be refined by subdividing the cracking lamina through the thickness [16].

The above considerations lead to the following equation for the step difference between the interlaminar stresses τ_{xz} (5):

$$\tau_{xz}^{i,i+1} - \tau_{xz}^{i-1,i} = \sum_{j=1}^{N-1} [H_{ij}^{-1} - H_{i-1,j}^{-1}] [\hat{u}(j+1) - \hat{u}(j)] \quad (5)$$

where H_{ij} is the coefficient matrix [16]. Then, using the equilibrium equations (6):

$$\begin{aligned} \frac{\partial \hat{\sigma}_x}{\partial x} + \frac{\tau_{xz}^{i,i+1} - \tau_{xz}^{i-1,i}}{h_i} &= 0 \\ \sigma_y &= C(x) \\ \sigma_z &= 0 \end{aligned} \quad (6)$$

the system of ordinary differential equations can be obtained (7):

$$\left\{ \ddot{u}_i \right\} + [D]\{u_i\} = 0 \quad (7)$$

After rewriting [D] in terms of eigenvalues [A] and eigenvectors [V] we get an uncoupled system of ordinary differential equations (8):

$$\left\{ \ddot{Z}_i \right\} + [A]\{Z_i\} = 0 \quad (8)$$

A detailed derivation of the equations can be found in [16].

At that point the 1D problem is reduced to a characteristic equation, the solution of which results in a linear combination for the average displacements in lamina i :

$$\hat{u}_i = \sum_{j=1}^N V_{ij} Z_j \quad (9)$$

where

$$Z_i = r_i \exp(x\sqrt{-A_i}) + s_i \exp(-x\sqrt{-A_i}) \quad (10)$$

where r_i and s_i are constants to be found in terms of the boundary conditions, A_i are the eigenvalues, and V_{ij} are the eigenvectors in (8). In (10), all eigenvalues A_i are negative, so (10) it can be written as

$$Z_i = p_i \sinh(x\sqrt{-A_i}) \quad i = 1 \dots N \quad (11)$$

where $p_i = 2r_i$.

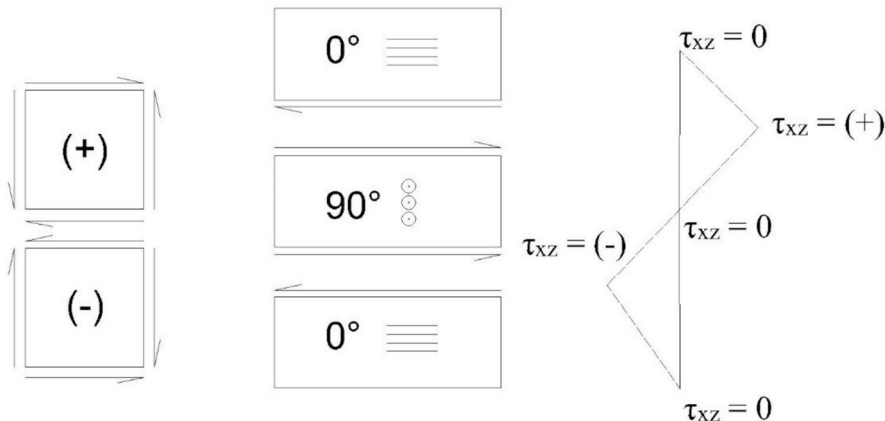


Fig. 2. Interlaminar stress distribution [16].

Let's consider one of the Z_i components, as shown on Fig. 3.

Fig. 3 shows that Z_S represents a homogeneous deformation (constant strain) for the case of a small eigenvalue A_S . It can be seen that in the interval $-l < x < l$, the plot is almost linear. Thus, for this particular component Z_S , the deformation (strain) is nearly homogeneous (constant). For the sinh function to become linear in the range $-l < x < l$, the eigenvalue A_S must be very small and the amplitude p_S very large, which leads to numerical problems. To solve this issue, the homogeneous deformations is approximated by a zero eigenvalue and a linear function $Z_S = x$. Then, the average displacements become:

$$\widehat{u}_i = \sum_{j=1}^N (1 - \delta_{js}) V_{ij} Z_j + \epsilon_x^0 x \tag{12}$$

where ϵ_x^0 is the constant strain corresponding to the homogeneous deformation.

In order to use the average displacement equation (12), it is necessary to obtain the constants p_i and ϵ_x^0 , which is done using the following boundary conditions for the RVE:

1. Homogeneous deformation on the boundary: The average displacement in every lamina (m) except for the cracking lamina (k), must be the same

$$\widehat{u}_m(\pm l) = \widehat{u}_r(\pm l); \forall m \neq k \tag{13}$$

where any lamina r without cracks is taken as reference.

2. Stress free crack surface: The cracking lamina (k) is subjected to zero stress because the cracks are on the boundary of the RVE at $\pm l$ (Fig. 1)

$$\int_{-\frac{1}{2}}^{\frac{1}{2}} \widehat{\sigma}_x^k(l) dy = 0 \tag{14}$$

where the integration limits represent the length in the y -direction (90°-fiber direction) for the RVE.

3. External load: The load is applied to the entire laminate except for the cracking lamina, because there is a free surface at $x = \pm l$ (Fig. 1)

$$\sum_{i=1}^N (1 - \delta_{ik}) h_i \int_{-\frac{1}{2}}^{\frac{1}{2}} \widehat{\sigma}_x^i(l) dy = N_x = h \widehat{\sigma}_x \tag{15}$$

where $h = \sum_{i=1}^N h_i$ is the thickness of the symmetric half of the laminate, k is the cracking lamina (90°-fiber direction in this case), δ is the Kronecker symbol, and $\widehat{\sigma}_x$ without a superscript is the average stress applied to the laminate.

Once the average displacement is found, the reduced stiffness E_x can be calculated using (2). The calculated reduced stiffness is used to obtain the crack density λ .

For a crack to grow, the Griffith/Irwin condition must be met [18]:

$$G_I(\lambda) \geq G_{Ic} \tag{16}$$

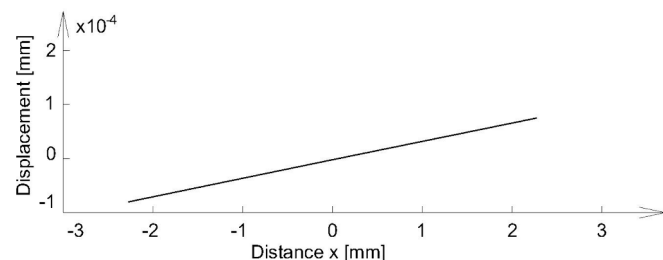


Fig. 3. Elemental function of Z_S for small eigenvalue A_S .

where G_{Ic} is the critical value of the Energy Release Rate (ERR) in mode I.

The value of the Energy Release Rate (ERR) for the case of uniaxial loading is obtained by [22, Eq.18].

$$G_I = \left(-\frac{t}{h_k} \frac{\Delta E}{2\Delta\lambda} \right) \epsilon_x^2 \tag{17}$$

where t is the thickness of the laminate, h_k is the thickness of the cracking lamina, and $\Delta E = E(2\lambda) - E(\lambda)$ is the difference between degraded laminate moduli for two successive crack states: λ and 2λ . The ERR $G_I(N)$ as a function of number of cycles can thus be calculated using (17). Then, the ERR can be used to characterize the damage-nucleation function $f(N)$ that represents the state of the material with respect to fatigue.

3. Fatigue analysis framework

Quasi-static damage in the laminate takes place either after the first fatigue cycle (N_1) or after a finite number of cycles (N_i). At that point in the life N_i of the specimen, the material reaches an equilibrium state where the applied energy release rate (G_I) is equal to the critical ERR G_{Ic} (i.e., the quasi-static fracture toughness). Any repetition of the load excursion does not lead to further damage because, as soon as the material damages, the ERR becomes less than the associated fracture toughness G_{Ic} of the material. In other words, the damage activation condition (16) is no longer met.

Under fatigue loading, even at constant amplitude, new defects arise and coalesce into new cracks. This process is controlled by hydrostatic stress in vicinity of micro-level defects. In this way, the crack-densities keep on growing during cycling, and for modelling purposes, this may be interpreted as degradation of the fracture toughness G_{Ic} of the material. The proposed equation for degradation of fracture toughness with cyclic loads application is [27, (11.7), (11.9)] is:

$$G'_{Ic} = G_{Ic} f(N); 0 < f(N) < 1 \tag{18}$$

In equation (18), G'_{Ic} is the fatigue fracture toughness, N is the number of cycles, and $f(N)$ is the defect-nucleation function, controlled by stress.

At any given number of cycles N during fatigue loading, the increase in crack densities requires the Griffith/Irwin condition to be met: $G'_{Ic} = G_I$. The current fracture toughness G_I can be evaluated at any known crack-density λ using (17) and then, the defect-nucleation function $f(N)$ can be derived [27, Ch. 11] as the quotient of the fatigue fracture toughness and the quasi-static fracture toughness values:

$$f(N) = \frac{G'_I}{G_{Ic}} \tag{19}$$

Using experimental data for thermal fatigue, processed through equation (19), the defect-nucleation function $f(N)$ for thermal fatigue was approximated by [(11.9) in [27]] in terms of the defect-nucleation rate β :

$$f(N) = 1 - \beta \log N; \beta > 0 \tag{20}$$

The fatigue analysis framework developed in [27] applies to composite materials loaded by temperature cycles only. In the present study, the fatigue analysis framework from [27] is applied to the case of composite materials under stress-controlled loading cycles. Application to a stress-controlled situation requires modification of the equations in [27], which impacts the results (see Section 5.2), as follows:

$$f(N) = 1; N < N_{th} \\ f(N) = a - \beta \log(N); N \geq N_{th} \tag{21}$$

where N_{th} is the defect-nucleation threshold, indicating the number of cycles when defect-nucleation begins, and a is the ordinate at the origin

of the defect-nucleation function. This is similar to metal fatigue, where the High Cycle Fatigue (HCF) S-N line runs above the Low Cycle Fatigue (LCF) line. Furthermore, N_{th} is similar to the transition life N_T where the LCF and HCF lines intersect in the S-N diagram.

4. Material identification procedure

The input data for the identification procedure is based on modulus degradation data $E_x(N)$ (Fig. 4).

The purpose of the identification procedure is to obtain a set of crack densities for all laminas that corresponds to a laminate modulus in the direction of load E_x^{DDM} that approximates the experimental value E_x^{exp} for the entire range of fatigue life N . The objective function is chosen as follows:

$$R_i = \sqrt{\left(\frac{E_{x,i}^{DDM} - E_{x,i}^{exp}}{E_{x,i}^{exp}}\right)^2} \quad (22)$$

where $i = 1 \dots n$, and n is the number of experimental data points (Fig. 4).

The proposed minimization procedure can be described as follows:

1. Get the first experimental value of laminate moduli E_{x1}^{exp} .
2. Assume a crack density $\lambda_{1,1}$ for the first iteration.
3. Evaluate the elastic modulus of the laminate E_{x1}^{DDM} using DDM equations (2), (13)–(15).
4. Calculate the objective function R (22). If its value is within the prescribed tolerance, then advance to step 6. If not, the optimizer must reevaluate the crack density for the next iteration using Nelder-Mead algorithm [37]. Then, repeat steps 2–5 until the objective function becomes smaller than a predetermined tolerance ($R \leq 0.005$). The positive aspect of the Nelder-Mead algorithm is that the function to be minimized doesn't need to have a derivative of any order, which is the case for DDM-based objective function in Eq. (22). The negative aspect of the Nelder-Mead algorithm is that it may require more attempts to converge in comparison with gradient based methods. In this work, no such convergence issues were found during data processing using the Nelder-Mead algorithm.
5. Converged values of crack densities for the current experimental point are selected as the minimum possible crack-density value for the next iteration.
6. The next experimental point E_{x2}^{exp} is taken. The iterative process to find the crack density λ_2 is conducted as in steps 2–5, with minimum possible crack density evaluated at step 6, until the required level of minimization of the objective function is achieved.
7. The minimum possible crack density is updated.

8. The rest of experimental points are processed using steps 1–8 until the optimum crack densities for all n experimental points are obtained.

The calculated crack densities λ are used to calculate the fatigue fracture toughness G'_{fc} using equation (17), and then, the defect-nucleation rate β is calculated using a linear approximation of $f(N)$ with respect to N in the form shown in (21). The applied strain ε to be used in equation (16) is calculated using the applied known experimental stress σ and the degraded modulus $E_x(\lambda)$ calculated for each point in the loading history.

For the considered lay-up, crack density accumulation is dominated by the defect-nucleation phenomenon, which has a physical meaning. Therefore, crack density accumulation is directly related to elastic modulus degradation.

5. Validation

5.1. Experimental data

To illustrate the proposed method, recently published experimental results were used [7,8] that provide comprehensive experimental data for the fatigue process in CFRP cross-ply specimens, including S-N curves, E-N curves, crack density versus number of cycles, and crack density versus stiffness degradation.

The first dataset [7], includes seven specimens made of unidirectional (UD) Prepreg Hexply F6376c-HTS(12K)-5–35 % with $[0_2/90_4]_s$ lay-up. These were tested under tension–tension fatigue loading with stress ratio $R = 0.1$. UD lamina properties are shown in Table 1.

The fatigue tests were performed at room temperature, with sinusoidal loading with peak stress of 507 MPa (70 % of ultimate tensile strength (UTS)), stress ratio $R = 0.1$, and frequency 5 Hz. At the end of each 500-cycle interval of loading–unloading, a ramp with a rate of 19 kN/s was applied to measure stiffness degradation. To measure crack density, the edge surface of each specimen was covered with white paint and shot by two cameras. Obtained photos were processed with MATLAB image-analyses code to count cracks in 90-degree plies.

The second dataset [8] included $[0_2/90_4]_s$ and $[0/90_2]_s$ layouts. The dimensions and material were identical to those of the first set. Specimens with $[0_2/90_4]_s$ lay-up were subjected to peak stress levels at 74, 70, 66, 63 % of UTS and specimens with $[0/90_2]_s$ lay-ups at 77, 70, 63 % of UTS. UTS was obtained experimentally from quasi-static tests conducted before the fatigue tests. The fatigue testing conditions were the same as for the first test.

Digital image correlation (DIC), acoustic emission (AE), and camera shooting systems were used together to collect data about crack density, as well as delamination onset and evolution. Also, stiffness degradation and Poisson's ratio evolution data were collected.

For validation of the proposed method, data of specimens with $[0_2/90_4]_s$ lay-up from both datasets are used in this work.

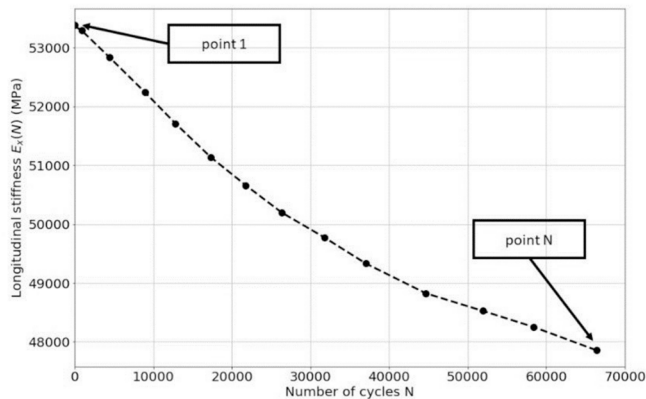


Fig. 4. Example experimental $E_x(N)$ curve. Data from [7], labelled “data-3” in Figs. 5 and 6.

Table 1
Monolayer material properties [7].

Parameter	Value
Longitudinal modulus	$E_{11T} = 142GPa$
Transverse modulus	$E_{22T} = E_{33T} = 9.1GPa$
In-plane shear modulus	$G_{12} = G_{13} = 5.2GPa$
Transverse shear modulus	$G_{23} = 3.5GPa$
Longitudinal strength	$X_T = 2274MPa, X_c = 1849MPa$
Transverse strength	$Y_T = 102MPa, Y_c = 255MPa$
In-plane shear strength	$S_{12} = S_{13} = 63MPa$
Transverse shear strength	$S_{23} = 35MPa$
In-plane Poisson ratio	$\nu_{12} = \nu_{13} = 0.27$
Ply thickness	$t = 0.125mm$

5.2. Results and discussion

The key part of the validation is to first assure that the DDM framework presented above is capable of mimicking the degradation of elastic modulus as a function of crack density $\frac{E_x}{E_{x0}}(\lambda)$ from experimental data. The results are shown on Fig. 5.

It can be seen in Fig. 5 that the analytical DDM solution closely follows the trend of the experimental data up to a point, sometimes for the entire range of crack density (data-3, data-19, etc.) but sometimes only from zero to some intermediate value of crack density. However, for most specimens, a threshold is observed beyond which the experimental $\frac{E_x}{E_{x0}}(\lambda)$ values start to deviate significantly from the DDM prediction (straight line). This can be explained by the initiation and propagation of delaminations, which were captured and reported in the experiments. Indeed, the comparison with experimental data for delamination onset shows (see Table 2), that in most cases, the deviation of experimental $\frac{E_x}{E_{x0}}(\lambda)$ data from DDM prediction corresponds to the onset of delamination. In Table 2, the value of the crack density λ , at which deviation starts (visually estimated from Fig. 5), was used to find the cycle number (delamination onset N_d) at which this crack density was achieved in the experiment [7,8]. Then, interlaminar crack ratio, defined in [7,8] as the average of maximum observed delamination lengths on the left and right sides of the specimen divided by the gauge length (~80 mm), was used to define the delamination onset cycle number from the experiment.

Next, the procedure for cyclic damage quantification proposed in the current study is further applied to the specimens having the most prolonged and close to analytical DDM $\frac{E_x}{E_{x0}}(\lambda)$ prediction range. The selected data are shown on Fig. 6.

After the confirmation step described above, the proposed procedure for cyclic damage quantification using DDM is implemented. At first, the crack densities for the corresponding elastic moduli from one of the experiments (Figs. 5 and 6, Experimental data-19) were derived using the proposed minimization procedure, as explained in Section 5. The results of the minimization, including R , are summarized in Table 3.

Experimental $E_x^{exp}(N)$ for the “data-19” dataset is shown in Fig. 4. For the same dataset, the calculated crack density in the 90-degree lamina is shown in Fig. 7. The increase in crack density versus N is gradual and then it becomes faster, in the case of Fig. 7 at $N \approx 58000$ when the crack

Table 2

Comparison of delamination onset cycles from experiment and method valuation data.

Experimental data	Lay-up	Maximum cyclic stress, MPa	N at delamination onset from comparison of DDM and experimental $\frac{E}{E_0}(\lambda)$, cycles	N at delamination onset from experiment [7,8] cycles
7	[0 ₂ ,	507	21,966	25,068
15	90 ₄] _s	453	61,812	57,086
17		507	9310	12,827
2		507	12,397	11,197
11		480	24,726	27,913

density λ is about 1.25 mm⁻¹. In Fig. 7, the number N was taken from experiment, and the crack density is calculated by the proposed methodology.

The results on Fig. 7, supported by Table 3, aim only to show an example of the proposed methodology used to calculate the elastic moduli as proposed in this work. In Table 3, it can be seen that predicted and experimental values of laminate modulus agree for the whole range of fatigue life ($N = 0-66,386$). Also, it can be seen in Table 3 and Fig. 7 that, for the available range of experimental crack density data ($N = 0-17,301$), comparison between prediction and experimental data is good. The quality of the predicted crack density all the way up to the highest life $N = 66,386$ is advocated on the fact that DDM provides a bi-univocal relationship between laminate E and laminae crack densities. Such accuracy is supported by comparison to quasi-static experiments in [16–19,22–24,27]. DDM’s accuracy is based on its analytical solution of the deformation in all laminas, including the perturbations introduced by each crack.

Next, the experimental fatigue performance of the selected specimens is considered. The defect-nucleation function is obtained using Eq. (18), (19), (21) and the results are shown on Fig. 8. The crack-density λ is known, as calculated by the minimization procedure. The applied strain ε was calculated using applied stress σ (constant, from experiment) and degraded modulus $E_x(\lambda)$ calculated by the proposed methodology, for each point in the loading history. Finally, the ERR G_I , and the defect-nucleation function $f(N)$ can all be calculated using (18), (19), (21).

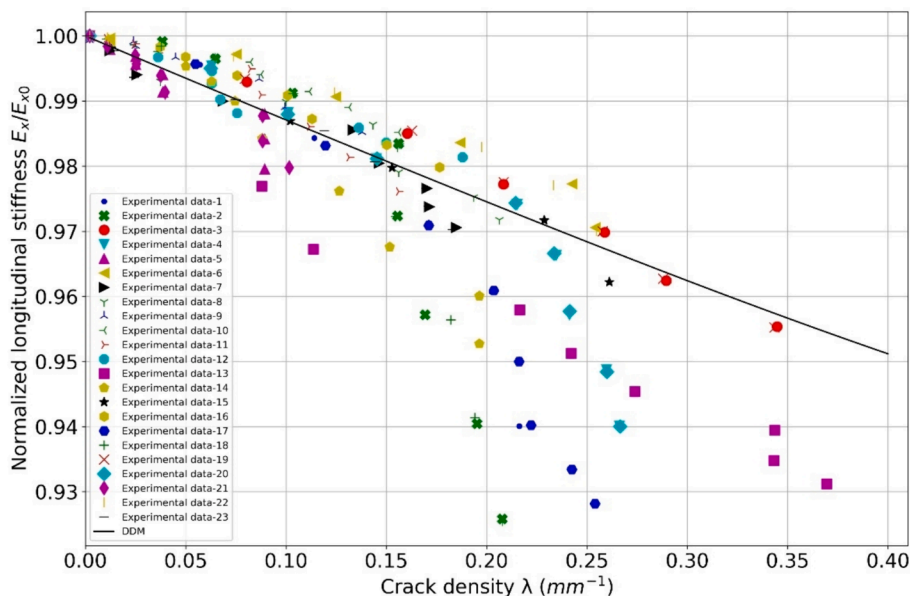


Fig. 5. Comparison of DDM informed and experimental normalized stiffness degradation of the laminate $\frac{E_x}{E_{x0}}$ with respect to accumulated crack density $\lambda[1/mm]$ during stress-controlled fatigue experiments.

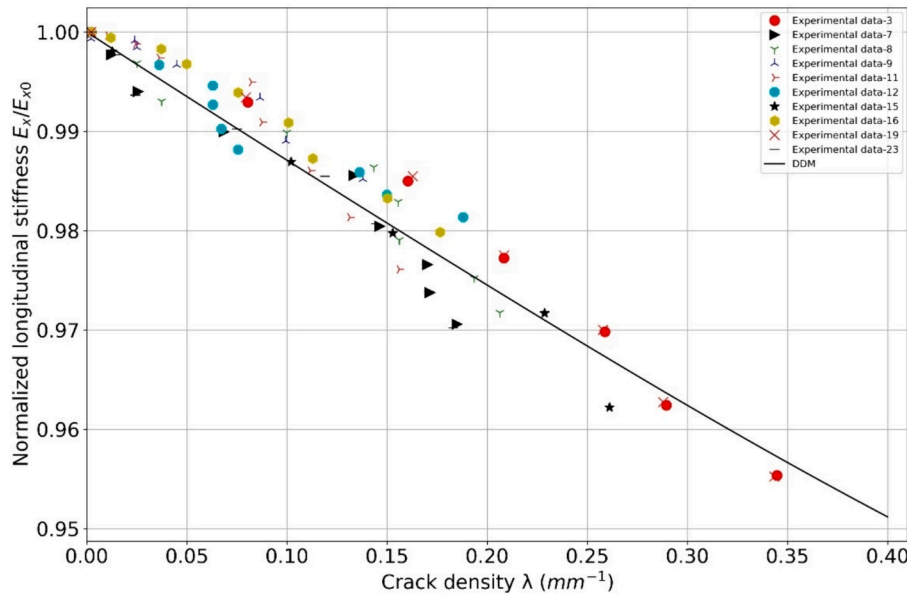


Fig. 6. Selected experimental data for the analysis of cyclic damage quantification using the proposed framework.

Table 3

E_x^{exp} is the longitudinal elastic modulus from experiment, E_x^{DDM} is obtained using the proposed minimization procedure, λ^{exp} is the crack density from experiment, λ^{DDM} is obtained using the proposed minimization procedure, and R is the objective function value (22).

Point #	N , cycles	E_x^{exp} , MPa	E_x^{DDM} , MPa	R	λ^{exp} , mm^{-1}	λ^{DDM} , mm^{-1}
1	0	53,385	53,367	0.000345	0	0.010
2	885	53,295	53,295	4.33E-10	0.027	0.016
3	4460	52,833	52,833	1.04E-10	0.120	0.087
4	8930	52,245	52,245	3.26E-10	0.208	0.179
5	12,831	51,711	51,711	4.55E-10	0.265	0.265
6	17,301	51,141	51,141	2.89E-10	0.314	0.361
7	21,770	50,661	50,661	1.91E-10	-	0.449
8	26,321	50,200	50,200	1.82E-10	-	0.543
9	31,766	49,775	49,775	1.88E-10	-	0.644
10	37,048	49,331	49,331	9.03E-11	-	0.773
11	44,687	48,825	48,825	1.20E-10	-	0.969
12	51,920	48,526	48,526	4.55E-11	-	1.131
13	58,340	48,255	48,255	2.85E-11	-	1.334
14	66,386	47,857	47,857	2.45E-11	-	1.859

As Fig. 8 suggests, the defect-nucleation function $f(N)$, and hence the fatigue fracture toughness G_{Ic} , is nearly constant (equal to one) up to $N \approx 3 \times 10^3 \dots 4 \times 10^4$ depending on the specimen. The upper limit of the number of load cycles N_{th} quoted above could be called “defect-nucleation threshold”, to highlight the threshold number cycles after which the quasi-static fracture toughness G_{Ic} starts to degrade under stress-controlled cyclic loading.

Such performance differs from earlier observation for thermal fatigue [27], where the defect-nucleation function $f(N)$ started to decrease after just a few cycles. The observed phenomenon in this work, namely a retardation of the defect-nucleation function $f(N)$ evolution may be explained as follows.

Thermal cycling produces thermal strain cycles, and the magnitude of the thermal strain decreases with modulus reduction that invariably happens as the crack density increases. Such reduction of thermal strain precludes further crack density growth. Thus, in thermal fatigue, crack density can increase only due to defect-nucleation, as defect-nucleation reduces the fatigue fracture toughness. In other words, under thermal cycling (or strain driven fatigue tests for that matter) no crack density growth can happen unless the defect-nucleation increases. Thus, the

defect-nucleation function starts to increase (β is negative in (20)) as soon as the first crack appears.

On the contrary, stress driven fatigue (as in [7,8]) does increase the strain immediately with any modulus reduction caused by increased crack density. Since stress is constant, any damage results in modulus reduction and immediate strain increment. Then, as long as the strain is increasing, it is not absolutely necessary to rely on defect-nucleation to produce new cracks. Thus, the defect-nucleation may remain null ($\beta = 0$) while crack density is increasing, but only to a point, which is denoted by the proposed defect-nucleation threshold (N_{th}).

In the region $0 < N < N_{th}$, using (17), the calculated ERR is $G_I = 0.472 N/mm$ for the test data chosen (data-19). Due to the assumption explained in Section 4, this value is equal to the quasi-static critical energy release rate G_{Ic} . After N_{th} cycles, the only way to fit the data in Fig. 8 is to let the defect-nucleation increase (beta negative). In the proposed analytical model, the region of increase in defect-nucleation function is approximated by a linear dependency between $f(N)$ and base $10 \log N$.

The defect-nucleation rate β was obtained for several specimens from the selected datasets. Only data before delamination is used. Only three datasets were amenable for analysis with (21) and thus reported in Table 4. The remaining datasets terminate abruptly before defect-nucleation rate β can be detected.

As it follows from Table 4, the defect-nucleation rate β values have a scatter of about 4 % and no strong dependency on load, which advocates it as a proper material parameter to describe the fatigue related processes in composite materials.

Also, the results confirm the ability of the proposed method to describe cyclic damage with suitable parameters.

It is also noted from Table 4 that the form of damage nucleation function $f(N)$ is different from the one from for thermal fatigue study (20), i.e., strain controlled. This result is a direct consequence of stress-controlled fatigue loading, with consequent identification of the defect-nucleation threshold N_{th} .

Furthermore, due to appearance of delaminations, the damage nucleation function $f(N)$ for stress-controlled loading should be used only in its effective range of cycles $N = [0, N_d]$.

The proposed method calculates crack density λ by minimizing the error between the modulus calculated by DDM E_x^{DDM} and the experimental value E_x^{exp} obtained during fatigue testing. Ply material properties and LSS are also needed. Furthermore, the defect-nucleation

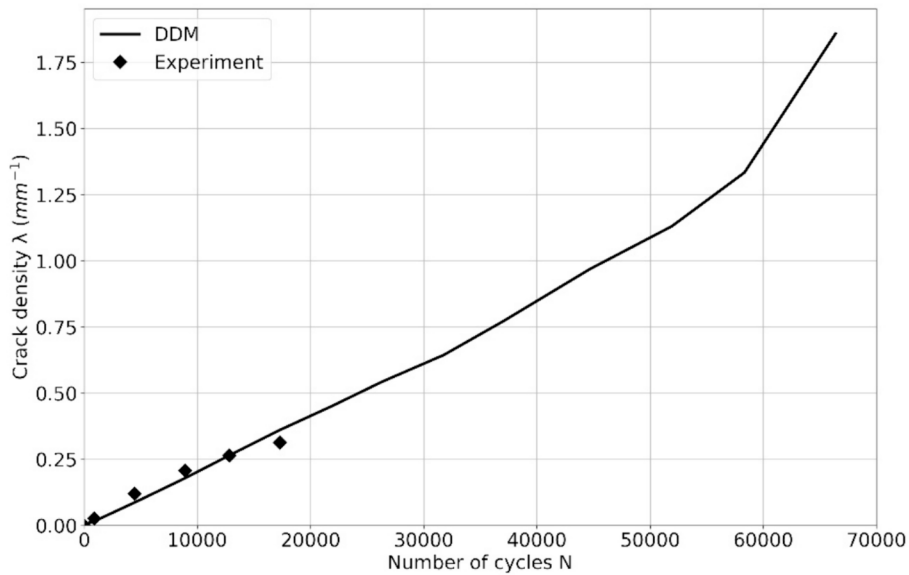


Fig. 7. Crack density accumulation $\lambda(N)$ calculated by the proposed methodology.

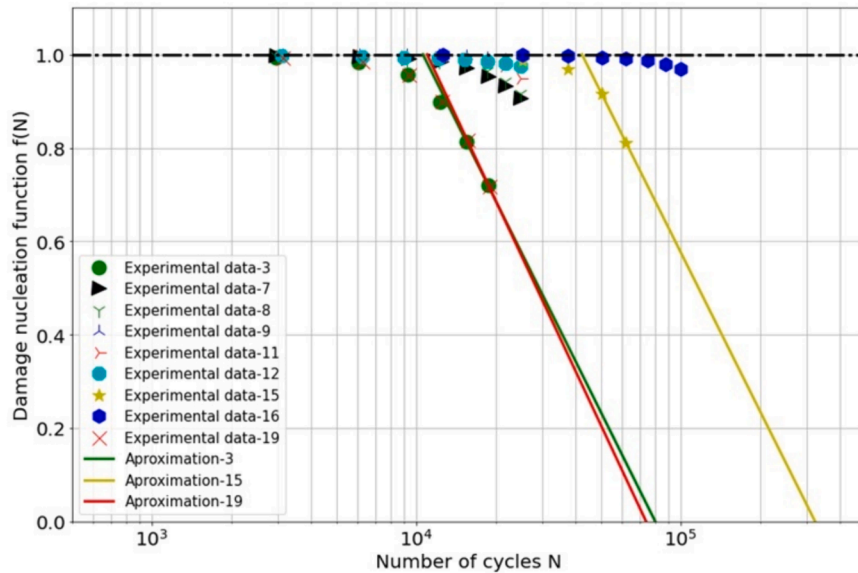


Fig. 8. Defect-nucleation function $f(N)$ during fatigue loading.

Table 4

Defect-nucleation rates, thresholds, and functions, for selected specimens.

Experiment #	Lay-up	Maximum cyclic stress, MPa	Defect-nucleation threshold, N_{th} , cycles	Defect-nucleation rate, β	Defect-nucleation function, $f(N)$ (21)
3	[0 ₂ ,90 ₄] _s	507	6×10^3	1.134	$5.58-1.134\log N$
15		453	2×10^4	1.123	$6.25-1.123\log N$
19		507	6×10^3	1.203	$5.88-1.203\log N$

function $f(N)$ (21) with parameters β and N_{th} are needed and obtained from the same experimental data, recast into Fig. 8. Also in Fig. 8, at $N \rightarrow 0$, $f(0) \rightarrow 1$, and $G'_{Ic} = G_{Ic}$, so that (19) provides the quasi-static fracture toughness G_{Ic} . Furthermore, in Fig. 8, defect-nucleation starts at N_{th} , thus allowing to find N_{th} from the same experimental data.

There are no material parameters adjusted during minimization. Minimization is used only to predict crack density $\lambda(N)$ excluding the necessity to measure it during fatigue testing. Through minimization,

the crack density is calculated and results in predicted stiffness degradation that will match the experimental stiffness degradation. The calculated and experimental values of both E_x and λ are compared in Figs. 5 and 6. The deviation of calculation from experiments in Fig. 5 allows us to detect when delaminations occur, as reported in Table 2.

In its current state, the proposed fatigue analysis framework cannot be used directly to model crack density accumulation for cases where delamination damage mode dominates, such as delamination during

compression after impact [40] and delamination onset [41]. Further development of the proposed analysis method will be addressed in future work.

6. Conclusions

In this study, a method for damage quantification based on experimental stiffness degradation data for composite laminates subjected to fatigue load is proposed. The framework of discrete damage mechanics is shown to provide valid predictions of crack density corresponding to experimental values of elastic moduli degradation. Furthermore, the framework provides an analytical expression to calculate the initial (quasi-static) fracture toughness and then, the fatigue fracture toughness as a function of life N and applied strain, even when such strain is calculated from the available experimental data of stress using the modulus data. Knowing the quasi-static and fatigue fracture toughness, it is then possible to calculate the fatigue-controlled defect-nucleation rate. Furthermore, an additional parameter is proposed in this study to identify the threshold life at which the defect-nucleation starts to occur. And finally, delamination onset can be detected by analyzing the deviation of the modulus-reduction experimental data from the linear decrement predicted by the analytical solution.

The procedure of minimization, based on Nelder-Mead algorithm, provides accurate results in finding the crack-density after known stiffness degradation for a range of points, where matrix cracking was the dominant damage mechanism. This fact simplifies the experimental work to just measuring modulus reduction rather than counting cracks, thus avoiding the experimental hurdles that the latter entails.

An additional parameter was introduced to characterize the fatigue performance of composite material, namely the number of cycles until the start of fracture toughness degradation, which was named “defect-nucleation threshold”. This parameter appears to be a peculiarity of stress-controlled fatigue loading, unlike strain-controlled loading where the defect-nucleation in the material initiates at the very beginning of the load history.

The defect-nucleation rates that were obtained in this study have a small scatter, thus advocating the defect-nucleation rate as a reasonable property for characterization of fatigue behavior of composite materials subjected to cyclic loading.

The effect of the delamination on the fatigue life of composites will be studied in future research. In the present form, fatigue crack density accumulation characterization by the proposed methodology can be achieved in the number of cycles ranging up to delamination onset.

CRediT authorship contribution statement

Nikolay V. Turbin: Writing – original draft, Validation, Software, Project administration, Methodology, Conceptualization. **Kirill A. Shelkov:** Writing – review & editing, Validation, Software, Data curation. **Nikolai O. Kononov:** Writing – review & editing, Data curation. **Ever J. Barbero:** Writing – review & editing, Supervision, Conceptualization.

Declaration of competing interest

The authors declare that they have no known competing financial interests or personal relationships that could have appeared to influence the work reported in this paper.

Data availability

Data will be made available on request.

Appendix A. Supplementary material

Supplementary data to this article can be found online at <https://doi.org/10.1016/j.compstruct.2024.118271>.

[org/10.1016/j.compstruct.2024.118271](https://doi.org/10.1016/j.compstruct.2024.118271).

References

- [1] Soutis C. Fibre reinforced composites in aircraft construction. *Prog Aerosp Sci* 2005.
- [2] Ussorio M. Development of matrix cracks in cross-ply laminates under bending and their detection using FBG sensors. University of Surrey (United Kingdom); 2004.
- [3] Lebedev MP, et al. The formation of microcracks during climatic aging of polymer-composite materials. *Polym Sci, Ser D* 2023;16:116–23.
- [4] Pascoe JA. Slow-growth damage tolerance for fatigue after impact in FRP composites: why current research won't get us there. *Theor Appl Fract Mech* 2021; 116:103127.
- [5] Molent L, Haddad A. A critical review of available composite damage growth test data under fatigue loading and implications for aircraft sustainment. *Compos Struct* 2020;232:111568.
- [6] Couty V, Berthe J, Deletombe E, Lecomte-Grosbras P, Witz JF, Brieu M. Comparing methods to detect the formation of damage in composite materials. *Exp Tech* 2023; 47(3):689–708.
- [7] Li X, Kupski J, De Freitas ST, Benedictus R, Zarouchas D. Unfolding the early fatigue damage process for CFRP cross-ply laminates. *Int J Fatigue* 2020;140: 105820.
- [8] Li X, Benedictus R, Zarouchas D. Early fatigue damage accumulation of CFRP Cross-Ply laminates considering size and stress level effects. *Int J Fatigue* 2022;159: 106811.
- [9] Kötter B, Endres J, Körbelin J, Bittner F, Endres HJ, Fiedler B. Fatigue and fatigue after impact behaviour of Thin-and Thick-Ply composites observed by computed tomography. *Compos Part C: Open Access* 2021;5:100139.
- [10] Shen H, Yao W, Qi W, Zong J. Experimental investigation on damage evolution in cross-ply laminates subjected to quasi-static and fatigue loading. *Compos B Eng* 2017;120:10–26.
- [11] Saeedifar M, Zarouchas D. Damage characterization of laminated composites using acoustic emission: a review. *Compos B Eng* 2020;195:108039.
- [12] Dvorak GJ, Laws N. *J Compos Mater* 1987;21:309329.
- [13] Singh BRT. Damage evolution under cyclic loading. In: *Advanced theories for deformation, damage and failure in materials*; 2012. p. 228.
- [14] Kassapoglou C. *Modeling the effect of damage in composite structures: simplified approaches*. John Wiley & Sons; 2015.
- [15] Kashtalyan M, Soutis C. Analysis of matrix crack-induced delamination in composite materials under static and fatigue loading. *Fatigue in Composites: Science and technology of the fatigue response of fibre-reinforced plastics*. Woodhead Publishing; 2003.
- [16] Barbero EJ, Barbero JC, Ugena CN. Analytical solution for plane stress/strain deformation of laminates with matrix cracks. *Errata Compos Struct* 2015;132: 621–32. <https://github.com/Echeban/Errata/blob/main/Errata133-COST-6508.pdf>.
- [17] Barbero EJ, Barbero JC. Analytical solution for bending of laminated composites with matrix cracks. *Compos Struct* 2016;135:140–55.
- [18] Barbero EJ, Cortes DH. A mechanistic model for transverse damage initiation, evolution, and stiffness reduction in laminated composites. *Compos B Eng* 2010;41 (2):124–32.
- [19] Moure MM, Sanchez-Saez S, Barbero E, Barbero EJ. Analysis of damage localization in composite laminates using a discrete damage model. *Compos B Eng* 2014;66:224–32.
- [20] Llobet J, Maimí P, Essa Y, de la Escalera FM. Progressive matrix cracking in carbon/epoxy cross-ply laminates under static and fatigue loading. *Int J Fatigue* 2019;119:330–7.
- [21] Hosoi A, Sakuma S, Fujita Y, Kawada H. Prediction of initiation of transverse cracks in cross-ply CFRP laminates under fatigue loading by fatigue properties of unidirectional CFRP in 90 direction. *Compos A Appl Sci Manuf* 2015;68:398–405.
- [22] Barbero EJ, Cosso FA. Determination of material parameters for discrete damage mechanics analysis of carbon-epoxy laminates. *Compos B Eng* 2014;56:638–46.
- [23] Adumitroaie A, Barbero EJ. Intralaminar damage model for laminates subjected to membrane and flexural deformations. *Mech Adv Mater Struct* 2015;22(9):705–16.
- [24] Blazquez AA, Matesanz MH, Ugena CN, Barbero EJ. Acoustic emission characterization of intralaminar damage in composite laminates. *MATCOMP* 2013; 13:33–8.
- [25] Kobayashi S, Takeda N. Experimental and analytical characterization of transverse cracking behavior in carbon/bismaleimide cross-ply laminates under mechanical fatigue loading. *Compos B Eng* 2002;33(6):471–8.
- [26] Morokov E, Levin V, Ryzhova T, Dubovikov E, Petronyuk Y, Gulevsky I. Bending damage evolution from micro to macro level in CFRP laminates studied by high-frequency acoustic microscopy and acoustic emission. *Compos Struct* 2022;288: 115427.
- [27] Barbero EJ. *Finite element analysis of composite materials using Abaqus®*. –. CRC Press; 2023.
- [28] Movahedi-Rad AV, Keller T, Vassilopoulos AP. Interrupted tension-tension fatigue behavior of angle-ply GFRP composite laminates. *Int J Fatigue* 2018;113:377–88.
- [29] Movahedi-Rad AV, Keller T, Vassilopoulos AP. Creep effects on tension-tension fatigue behavior of angle-ply GFRP composite laminates. *Int J Fatigue* 2019;123: 144–56.
- [30] Strizhius V. Predicting the degradation of the residual strength in cyclic loading of layered composites. *Mech Compos Mater* 2022;58(4):527–36.
- [31] Shokrieh MM, Lessard LB. Progressive fatigue damage modeling of composite materials, part I: modeling. *J Compos Mater* 2000;34(13):1056–80.

- [32] Van Paepegem W. Development and finite element implementation of a damage model for fatigue of fibre-reinforced polymers. Ghent University; 2002. Ph.D. thesis.
- [33] Degrieck J, Van Paepegem W. Fatigue damage modeling of fibre-reinforced composite materials. *Appl Mech Rev* 2001;54(4):279–300.
- [34] Brunbauer J, Pinter G. On the strain measurement and stiffness calculation of carbon fibre reinforced composites under quasi-static tensile and tension-tension fatigue loads. *Polym Test* 2014;40:256–64.
- [35] Brunbauer J, et al. Stiffness based fatigue characterisation of CFRP. *Adv Mat Res* 2014;891:166–71.
- [36] Hack M, Carrella-Payan D, Magneville B, Tadashi Naito U, Urushiyama TY, Yamazaki W, Van Paepegem W. A progressive damage fatigue model for unidirectional laminated composites based on finite element analysis: theory and practice. *Frattura Ed Integrità Strutturale* 2017.
- [37] Gao F, Han L. Implementing the Nelder-Mead simplex algorithm with adaptive parameters. *Comput Optim Appl* 2012;51(1):259–77.
- [38] Vassilopoulos AP, Keller T. Fatigue of fiber-reinforced composites. Springer Science & Business Media; 2011.
- [39] Nijssen RPL. Phenomenological fatigue analysis and life modelling. In: Vassilopoulos AP, editor. Phenomenological fatigue analysis and life modelling, Fatigue life prediction of composites and composite structures. Woodhead Publishing Limited and CRC Press LLC.; 2010.
- [40] Biagini D, Pascoe J-A, Alderliesten R. Investigation of compression after impact failure in carbon fiber reinforced polymers using acoustic emission. *J Compos Mater* 2023;57(10):1819–32.
- [41] Dávila CG, Joosten MW. A cohesive fatigue model for composite delamination based on a new material characterization procedure for the Paris law. *Eng Fract Mech* 2023;284:109232.